Electrolyte and SEI Decomposition Reactions of Transition Metal Ions Investigated by On-Line Electrochemical Mass Spectrometry

Sophie Solchenbach, *,z Gloria Hong, Anna Teresa Sophie Freiberg, Roland Jung, and Hubert A. Gasteiger**

Chair of Technical Electrochemistry, Department of Chemistry and Catalysis Research Center, Technical University of Munich, Garching, Germany

We use on-line electrochemical mass spectrometry (OEMS) to elucidate and quantify the electrolyte reduction on graphite caused by transition metal ions. To have a controlled system, we use ethylene carbonate (EC) with 1.5 M $LiPF_6$ and representative amounts of $Ni(TFSI)_2$ or $Mn(TFSI)_2$ as model electrolytes, combined with a 2-compartment cell in which anolyte and catholyte are separated by an impermeable solid lithium ion conductor. Focusing on C_2H_4 evolution as a marker for EC reduction, we find that both Ni^{2+} and Mn^{2+} lead to enhanced gas evolution on pristine graphite electrodes once the potential is decreased to below the TM^{2+}/TM^0 redox potential, demonstrating that the reduced transition metals are active toward electrolyte reduction. If the electrodes are preformed in a TM-free electrolyte and subsequently cycled in an electrolyte containing either Mn^{2+} or Ni^{2+}, the activity of nickel toward electrolyte decomposition is greatly reduced, whereas the electrolyte with manganese still shows a strong ongoing C_2H_4 generation. The use of vinylene carbonate during formation partially suppresses the gas evolution from manganese. Using OEMS and post-mortem ATR-FTIR, we finally show that reduced manganese can decompose organic SEI components into Li_2CO_3, thereby compromising the integrity of the SEI and enabling the additional reduction of electrolyte.

 [DOI: 10.1149/2.0511814jes]

Manuscript submitted August 30, 2018; revised manuscript received October 11, 2018. Published October 23, 2018.

Transition metal (TM) dissolution is a long-known degradation phenomenon of lithium manganese spinel-type cathode active materials for Li-ion batteries. It is amplified by temperature,[1,2] high cathode potentials,[3] and large BET surface area of the particles.[3] As layered lithium nickel cobalt manganese oxide (NCM) cathode materials are cycled to higher cutoff potentials to maximize the energy density of Li-ion cells, transition metal dissolution also becomes significant for NCMs.[4–11] Experimental and ab initio modeling studies suggest that the electrochemical oxidation of $LiPF_6$-based electrolytes at high voltages[8,12–17] and/or follow-up reactions of the electrolyte with oxygen released from the NCM host lattice[18–22] can generate HF, which then corrodes the layered transition metal oxide cathode materials. Upon lattice oxygen release (occurring upon delithiation to ~80% in NCMs),[18,19] not only manganese, but also nickel and cobalt are dissolved as TM^{2+} ions into the electrolyte[4] at concentration ratios that reflect the stoichiometry of the bulk material.[5,7,23]

The most apparent consequences of transition metal dissolution are capacity and power fade.[3,6–9,24–28] However, the amount of dissolved cathode active material is typically less than 1%,[7,9,26,28–30] which is too low to explain the observed capacity losses. Instead, the transition metal ions deposit on the graphite anode, where they lead to a significant decrease of the coulombic efficiency and to a large increase in anode impedance.[5–7,9,24,25,31–34] It is not fully understood how transition metal ions can cause these detrimental effects, yet the negative impact of manganese on graphite anode capacity retention is considerably worse compared to nickel and cobalt.[5,7,31]

Recent studies have shown that Mn^{2+} ions exchange rapidly with Li^+ ions contained in the solid electrolyte interphase (SEI), as evidenced by soaking either preformed graphite electrodes[24,35,36] or single SEI compounds such as LiF or Li_2CO_3[25,37] in Mn^{2+}-containing electrolytes. Furthermore, Mn^{2+} ions were found to accumulate at the interface between organic (outer) and inorganic (inner) SEI in EC-based electrolytes without additives.[25,32,37,38] While some groups identified exclusively Mn(+II) species like $MnCO_3$ and MnF_2,[24,35,39–41] others found also reduced manganese in its 0 or +1 oxidation state on lithiated graphite.[33,38,42,43] Considering that nano-sized transition metal carbonates and -fluorides have been tested as conversion-type anode materials,[44–48] a reduction of these species in the SEI to metallic manganese seems likely. However, since the irreversible capacity on graphite anodes is typically 30–50 times higher than the capacity required for a 2-electron reduction of the accumulated manganese,[2,7,28] additional side reactions must be taking place, consuming active lithium. One proposed hypothesis is that reduced manganese in contact with electrolyte re-oxidizes to Mn^{2+} by simultaneously reducing solvent molecules,[4,33,39] as supported by DFT calculations from Han et al.[49] If then the Mn^{2+} ions can be reduced again, a catalytic cycle would be established by which active lithium would be lost continuously into the SEI. While this appears plausible, the question remains why manganese would not eventually be covered by SEI species that would prevent new solvent molecules from reaching the active TM center, and thus would stop the electrolyte reaction with the TM center. To resolve this question, Leung[50] and Joshi et al.[32] suggested that transition metals also decompose organic SEI species, thus compromising the passivating properties of the SEI.

Despite the many mechanistic insights gained by the above described studies, the nature of the electrolyte or SEI decomposition reactions associated with manganese deposited on graphite anodes remains unclear. Moreover, the number of analogous studies on the effect of nickel ions is limited,[31] although nickel is the most commonly dissolved transition metal from Ni-rich NCMs and NCA.[5,7] The scientific debate is further complicated, as the typical sample washing and/or drying steps required for conducting detailed ex-situ diagnostics like X-ray photoelectron spectroscopy (XPS), X-ray absorption spectroscopy (XAS) or scanning electron microscopy (SEM) can easily affect the transition metal oxidation state.[4,43] Therefore, the use of operando techniques for investigating the transition metal redox mechanism in the SEI has become imperative.

In this work, we use on-line electrochemical mass spectrometry (OEMS) to investigate the fundamental reactions of carbonate based electrolytes with nickel and manganese ions on a graphite anode. In order to mimic the effect of a typical dissolution of ~0.3 wt% of the cathode active material observed in the above discussed studies, we use an ethylene carbonate (EC)/$LiPF_6$ model electrolyte containing Mn^{2+} or Ni^{2+} ions at the corresponding amounts. To avoid deposition of the transition metal ions on the lithium counter electrode, we use a sealed 2-compartment cell setup, separating the working and counter electrode compartments by a lithium ion conducting solid electrolyte.[12] As ethylene is the major gaseous product of the reductive decomposition of EC,[51,52] we will especially focus on its evolution during formation and cycling of graphite electrodes in Mn- or Ni-containing electrolytes. Considering that in real lithium-ion cells, transition metal dissolution occurs predominantly after the battery formation process

*Electrochemical Society Student Member.
**Electrochemical Society Fellow.
zE-mail: sophie.solchenbach@tum.de

is completed, we also investigate the effect of manganese and nickel ions on graphite electrodes that were preformed in a TM-free electrolyte. Finally, we use attenuated total reflection Fourier-transformed infrared (ATR-FTIR) spectroscopy and OEMS to elucidate the reactions of transition metal ions with SEI species.

Experimental

Preparation of electrodes and electrolytes.—Graphite electrodes were prepared by mixing graphite (SLP30, 7 m^2_{BET}/g, Timcal, Switzerland) and polyvinyl difluoride (PVDF, Kynar HSV 900, Arkema, France) in a ratio of 95:5 with N-methyl-pyrrolidone (NMP, anhydrous, Sigma-Aldrich, Germany; ink solid content 40%) in a planetary mixer (Thinky Corp., USA) at 2000 rpm for 15 min. The ink was then coated onto a polyester separator (FS 24316, Freudenberg, Germany) and dried at 50°C for 10 h. Electrodes with 15 mm diameter were punched out, dried in a glass oven (Büchi, Switzerland) under dynamic vacuum at 120°C for 12 h and transferred into the glove box without exposure to air. The final electrodes had a loading of 6.1 ± 0.2 mg_{SLP30}/cm^2 (≡ 2.3 mAh/cm^2). Glassfiber and polyester separators were also dried at 120°C under dynamic vacuum prior to use.

Electrolytes were prepared by mixing $LiPF_6$ (BASF SE, Germany) with ethylene carbonate (EC, BASF SE, Germany) or dimethyl carbonate (DMC, BASF SE, Germany) to yield a 1.5 M $LiPF_6$ concentration. For preformation of graphite anodes with an SEI-forming additive, vinylene carbonate (VC, BASF SE, Germany) was added at a concentration of 2 wt% to the as-prepared DMC/$LiPF_6$ electrolyte. Manganese bis-(trifluorosulfonyl)imide ($Mn(TFSI)_2$, 99.5%, Solvionic, France) and nickel bis-(trifluorosulfonyl)imide ($Ni(TFSI)_2$, 97%, Alfa Aesar, United States) were dried under dynamic vacuum at 120°C for 3 days and added to the electrolytes to yield a metal concentration of 10 mM, corresponding to a total amount of 1.5 µmol in the cell or 0.85 $µmol/cm^2$ per geometric graphite electrode area (based on 150 µL electrolyte and ø15 mm electrodes). For a full-cell with our graphite anodes and a balanced cathode with a loading of 13.5 mg_{CAM}/cm^2 (≡2.2 mAh/g for a specific capacity of 165 mAh/g), the total amount of dissolved transition metal would translate to ∼3.4 mg_{TM}/g_{CAM} or ∼0.3 wt%.

On-line electrochemical mass spectrometry.—The online electrochemical mass spectrometry (OEMS) system and a standard one-compartment electrochemical cell have been described in our previous publication.[53] To avoid the deposition of TM ions on the Li metal counter electrode, a sealed 2-compartment cell was used, where working and counter electrode compartments are separated by an impermeable lithium-ion conductive glass ceramic (LICGC, Ohara Corp., Japan) with an aluminum foil edge-seal.[12,54] The counter electrode compartment, which is shielded from the OEMS inlet, contained the Li counter electrode (ø 17 mm, 450 µm thickness, Rockwood Lithium, United States) and a 22 mm diameter glass fiber separator soaked with 250 µL EC + 1.5 M $LiPF_6$ or DMC + 1.5 M $LiPF_6$ without any transition metal ions added. The working electrode compartment that is connected to the OEMS inlet contained the graphite working electrode (ø 15 mm) and a polyester separator (ø 17 mm), both soaked with 150 µL of the test electrolyte, i.e., with or without TM salts added. After connection to the OEMS inlet and a rest period at open circuit voltage (OCV) for 4 h, we performed cyclic voltammetry at a rate of 0.2 mV/s, starting from OCV (∼3 V vs. Li^+/Li) and then scanning between 0.1 V and 2 V or 3 V vs. Li^+/Li. For quantification of the mass spectrometer currents, a calibration gas containing H_2, O_2, CO_2, and C_2H_4 (each 2000 ppm) or H_2, O_2, CO_2, and CO (each 2000 ppm) in Argon (Linde AG, Germany) was used. All currents were normalized to the current at m/z = 36 (Ar isotope) in order to correct for effects of minor pressure and temperature deviations, and afterwards the currents m/z = 2 (H_2), m/z = 26 (C_2H_4), m/z = 28 (CO, corrected for contributions from C_2H_4 and CO_2 as described by Strehle et al.),[55] and m/z = 44 (CO_2) were converted into gas concentrations.

For experiments with preformed electrodes, graphite electrodes coated on polyester separator were cycled 2 times with a rate of C/8 (based on graphite capacity) vs. a LFP electrode (3.5 mAh/cm^2, Custom Cells, Germany) in EC/1.5 M $LiPF_6$ electrolyte between 3.45 and 2 V cell voltage. The preformed cells were then discharged to 0.3 V cell voltage (corresponding to a graphite potential ∼2.9 V vs. Li^+/Li) and held at this potential for 10 h. Subsequently, the cells were disassembled inside a glove box, and the graphite electrodes were transferred without further washing into another OEMS cell with freshly prepared electrolyte and separators. For the experiments with graphite electrodes stored/preformed in EC and cycled in DMC as well as for graphite electrodes preformed in DMC/1.5 M $LiPF_6$ + 2 wt% VC, the graphite electrodes were washed with 5 mL DMC prior to the assembly of the OEMS cell in order to remove any remaining electrolyte contained in the pores of the harvested graphite electrodes.

Attenuated total reflection fourier-transform infrared spectroscopy (ATR-FTIR).—For ATR-FTIR analysis, both LFP cathode and graphite anode from the preformed cells (cycled at C/8 in EC + 1.5 M $LiPF_6$ between 2.0–3.45 V_{cell}) were transferred into a new cell with fresh separators and electrolyte with/without transition metals, and cycled again for 2 cycles at C/8 between the same cell voltages. The cells were then disassembled inside an Ar-filled glove box. The graphite electrodes were washed with 1.5 mL DMC and dried for 20 min under dynamic vacuum in the glove box antechamber at room temperature. ATR-FTIR spectra of the electrodes were then measured inside the glove box using a Spectrum Two spectrometer (Perkin Elmer) with a resolution of 4 cm^{-1} with 128 scans on a MIRacle germanium ATR (Pike Technologies). The spectra were normalized to the intensity of the PVDF peak at 1190 cm^{-1} (-CF_2- stretching vibrations).[56]

Results

Pristine graphite electrodes.—As a first step, we investigate the effect of transition metal ions on the electrolyte decomposition reactions of pristine graphite electrodes, i.e., when no SEI is present. This represents the situation in commercial Li-ion cells prior to battery formation, where dissolved transition metals are observed upon electrolyte storage of the pristine materials,[26] likely formed by the reaction of cathode active materials with HF, which is present in commercial $LiPF_6$ based electrolytes at the level of several tens of ppm, or at even higher concentration if cell components are dried improperly.[57,58] As ethylene carbonate (EC) is reduced to mostly lithium ethylene dicarbonate (LEDC) and C_2H_4,[51,59–62] so that the latter is the main gaseous product during graphite SEI formation in EC-based electrolytes,[52,55,63] we first focus on C_2H_4 as a marker of the reductive decomposition of EC. Figure 1 shows the current density (a) and the integral C_2H_4 evolution (b), both normalized to the active material mass of the graphite electrode, during 4 CV cycles of pristine graphite electrodes in EC/$LiPF_6$ without added transition metal salts, or with either 1.5 µmol Mn^{2+} or 1.5 µmol Ni^{2+} added as TFSI salts (equating to ∼140 $µmol_{TM}/g_{Graphite}$, which would correspond to ∼0.3 wt% dissolution of a NCM cathode active material in a balanced full-cell; for details see Experimental section).

The blue lines in Figure 1 show the baseline for the transition metal-free electrolyte. During the first cycle, a reduction peak current around 0.5 V vs. Li^+/Li appears (Figure 1a), alongside with the evolution of ∼80 µmol/g C_2H_4 (Figure 1b), in good quantitative agreement with the ∼10 $µmol/m^2_{BET}$ C_2H_4 found in earlier studies on the same graphite (BET: 7 m^2/g).[12,55] In the following cycles, the C_2H_4 evolution stops (as indicated by the constant concentration), also consistent with our previous reports.[12,52,55,64] When 1.5 µmol $Ni(TFSI)_2$ are added to the electrolyte, an additional reduction feature in the first cycle, starting at ∼2.5 V vs. Li^+/Li, can be seen in the current response (see green line in Figure 1a). For the Ni-containing electrolyte, C_2H_4 is evolved at much less negative potentials in the first reduction cycle (at ∼1.6 V vs. Li^+/Li) and at higher amounts (112 µmol/g, see green lines in Figure 1b; for details please also refer

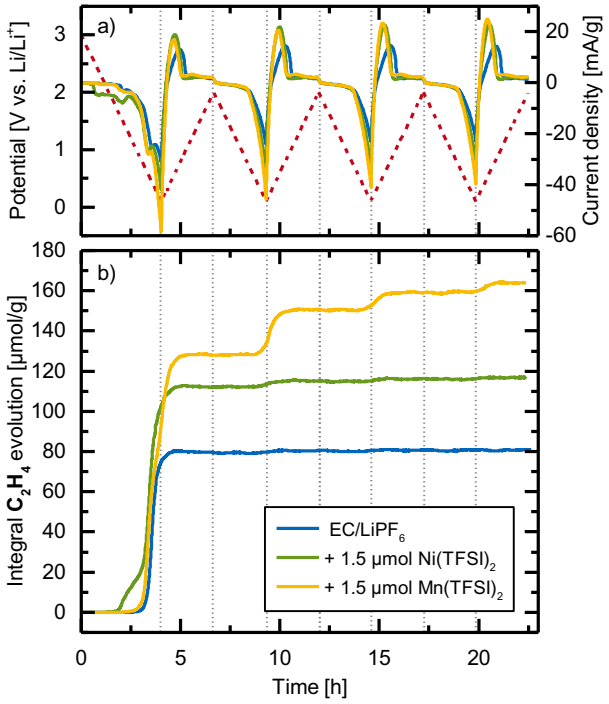

Figure 1. Currents and ethylene evolution during the first 4 voltammetric cycles of pristine graphite electrodes in EC/1.5 M $LiPF_6$ electrolyte without added metal salts (blue lines), with 1.5 µmol $Ni(TFSI)_2$ (green lines), or with 1.5 µmol $Mn(TFSI)_2$ (yellow lines). a) Currents normalized to graphite mass (solid lines) and potential (red dashed line); b) integral ethylene evolution normalized to graphite mass. The voltammetric cycles were conducted at 0.2 mV/s between 0.1–2.0 V vs. Li^+/Li, starting the first reductive scan from OCV (~3 V vs. Li^+/Li).

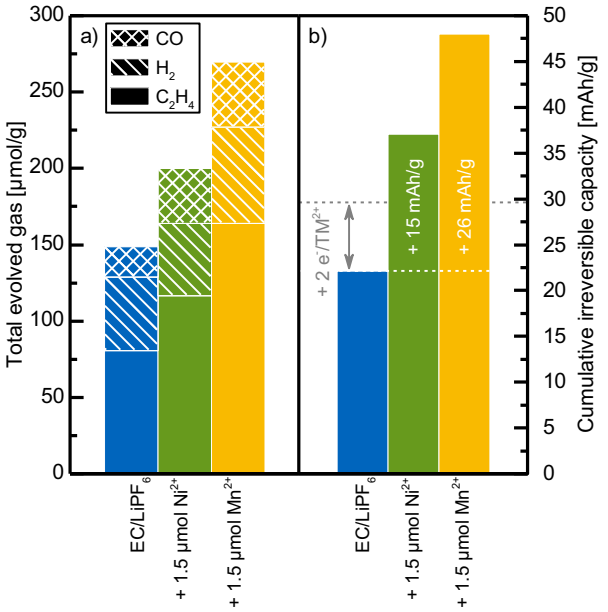

Figure 2. Total evolved gas and cumulative irreversible capacity (both normalized to graphite mass) over the first 4 cycles of the pristine graphite electrodes shown in Figure 1, i.e., in EC/1.5 M $LiPF_6$ electrolyte without added metal salts (blue bars), with 1.5 µmol $Ni(TFSI)_2$ (green bars), or with 1.5 µmol $Mn(TFSI)_2$ (yellow bars). a) Total evolved C_2H_4 (solid bars), H_2 (dashed bars), and CO (squared bars). b) Cumulative irreversible capacity, with the gray arrow indicating the theoretical charge for 2-electron reduction of the added Ni^{2+} or Mn^{2+} ions.

to Figure 5), which increases slightly up to 117 µmol/g by the end of 4 charge/discharge cycles. As previous studies showed an identical gassing behavior of graphite electrodes cycled in either transition metal-free LiTFSI[64] or $LiPF_6$[52,55] based electrolytes, the effect of the $TFSI^-$ anions on gassing should be negligible, so that the changes upon the addition of $Ni(TFSI)_2$ must be due to the presence of Ni^{2+}. The addition of 1.5 µmol $Mn(TFSI)_2$ (see yellow lines in Figure 1) leads to the highest C_2H_4 evolution in the 1st cycle, namely 128 µmol/g. Quite strikingly, with Mn^{2+}, a distinct C_2H_4 evolution is seen in each cycle, accumulating to 164 µmol/g C_2H_4 after 4 charge/discharge cycles. A more detailed discussion on the potentials at which the 1st cycle reduction current peaks and the onset of C_2H_4 evolution occur can be found in the Discussion section (see Figure 5).

While C_2H_4 is the main gaseous product from EC reduction, H_2,[12,51] CO,[55,62,65,66] and CO_2[63,65] are also commonly observed during the formation of graphite in carbonate-based electrolytes. The total quantities of C_2H_4, H_2, and CO after 4 cycles are shown in Figure 2a. After 4 cycles in the TM-free electrolyte (blue bars in Figure 2a), 48 µmol/g H_2 and 20 µmol/g CO have been evolved in addition to the 81 µmol/g of C_2H_4. For Ni^{2+}- and Mn^{2+}-containing electrolytes (green and yellow bars in Figure 2a), the concentration of CO is almost twice as high as in the TM-free electrolyte (36 and 43 µmol/g, respectively). In contrast, the amount of H_2 is similar in the absence and presence of dissolved transition metals (TM-free: 48 µmol/g; with Ni^{2+}: 47 µmol/g; Mn^{2+}: 63 µmol/g). While H_2 is the reduction product of trace water and/or HF in the electrolyte,[57,64] CO evolution has been ascribed to a direct 2-electron reduction of EC,[65–68] a minor pathway for EC reduction. Note that we also see small quantities of CO_2 (<20 µmol/g) during the first cycle of all experiments, which is however consumed during the subsequent cycles and thus does not appear in Figure 2.

Figure 2b shows the cumulative irreversible capacities (i.e., the summed-up differences between lithiation and delithiation capacity) after the 4 CV cycles depicted in Figure 1a. For the TM-free electrolyte (blue bars), the cumulative irreversible capacity is 22 mAh/g, which fits well to the expected formation losses of 7–10% of the initial capacity for graphite electrodes.[9] The cumulative irreversible capacity over 4 cycles in an electrolyte with Ni^{2+} ions (green bars) is significantly higher (37 mAh/g), but still smaller than that of the Mn^{2+}-containing electrolyte (48 mAh/g), which fits to the observation that the latter also exhibits the highest amount of evolved gas (Figure 2a). Note that the additional cumulative irreversible capacity losses in the Ni-containing and the Mn-containing electrolytes (+15 mAh/g and +26 mAh/g, respectively) substantially exceed the capacity of ~7.5 mAh/g required for a simple 2-electron reduction of the TM^{2+} ions (see horizontal gray dashed line in Figure 2b; based on the added salt concentration of 0.85 µmol/cm² and the graphite loding of 6.1 mg/cm²), namely by a factor of ~2 for Ni^{2+} and of ~3.5 for Mn^{2+}. This clearly indicates that at least the difference between the measured cumulative irreversible capacity and the theoretical charge for the TM ion reduction to the metal (i.e., the ~7.5 mAh/g) must have gone into the irreversible reduction of the electrolyte.

The results from Figure 1 and Figure 2 show that in the presence of TM ions, especially Mn^{2+}, strong additional electrolyte reduction takes place, consuming lithium and generating gas. As the composition of the evolved gas is comparable for all electrolytes, the fundamental reactions during SEI formation in TM-free and TM-containing electrolytes are apparently very similar. Moreover, the results demonstrate that manganese species continuously decompose electrolyte, whereas the activity of nickel species toward electrolyte reduction subsides much quicker.

Preformed graphite electrodes.—In commercial cells, the majority of transition metal dissolution occurs typically during cycling at high temperatures or voltages over extended periods of time. In this case, the SEI is already formed when the transition metal ions reach the anode. Therefore, we also investigate the effect of Ni^{2+} and

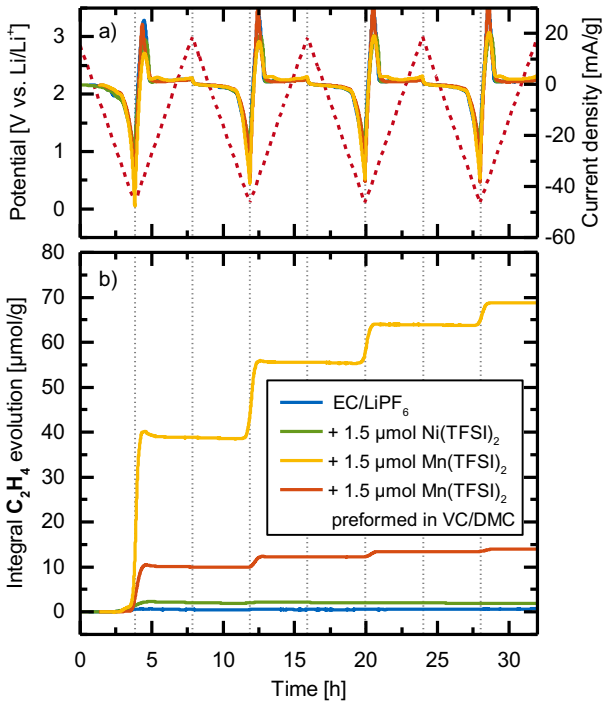

Figure 3. a) Currents and b) ethylene evolution, normalized to graphite mass, during the first 4 voltammetric cycles of preformed graphite electrodes in EC/1.5 M $LiPF_6$ electrolyte with/without added metal salts. Preformation was done with TM-free electrolyte in a separate cell vs. an LFP cathode (2 cycles at C/8), using two different preformation electrolytes: i) EC/1.5 M $LiPF_6$ for the OEMS experiments in TM-free electrolyte (blue) or electrolyte with either 1.5 µmol $Ni(TFSI)_2$ (green lines) or 1.5 µmol $Mn(TFSI)_2$ (yellow); ii) DMC/1.5 M $LiPF_6$ + 2% VC for the OEMS experiment in electrolyte with 1.5 µmol $Mn(TFSI)_2$ (orange). The voltammetric cycles at 0.2 mV/s were done between 0.1–3.0 V vs. Li^+/Li, starting from OCV (~2.9 V vs. Li^+/Li).

Mn^{2+} ions on preformed graphite electrodes. The SEI formation was achieved by pre-cycling (2 cycles at C/8) the graphite electrodes in a 1-compartment OEMS cell with capacitively oversized LFP counter electrodes in a TM-free EC + 1.5 M $LiPF_6$ electrolyte; the resulting SEI is known to consist mostly of LEDC and LiF, with only traces of Li_2CO_3 present.[60] Afterwards, the cells were deep-discharged to a cell voltage of 0.3 V_{cell} (corresponding to a graphite electrode potential of ~2.9 V vs. Li^+/Li), and the graphite electrodes were then transferred without further washing into the 2-compartment OEMS cell in an Ar-filled glove box. The discharge capacity over these first two formation cycles was 350–355 mAh/g, while the irreversible capacity accumulated to 25–27 mAh/g.

Figure 3 shows the current density (a) and the integral C_2H_4 evolution (b) during 4 CV cycles of the thus preformed graphite electrodes in electrolytes containing 1.5 µmol Mn^{2+} (yellow lines), 1.5 µmol Ni^{2+} (green lines) or no transition metal ions (blue lines). As one would expect, the TM-free electrolyte baseline for the preformed graphite electrode does no longer show the EC reduction current peak at ~0.5 V vs. Li^+/Li, consistent with the observation that only traces of C_2H_4 (~0.5 µmol/g) are evolved compared to the ~80 µmol/g C_2H_4 evolved on a pristine graphite electrode (blue line in Figure 1b). Hence, the passivating properties of the SEI preformed in EC/$LiPF_6$ remained largely intact after transferring the preformed graphite electrode into the 2-compartment OEMS cell. On the other hand, with 1.5 µmol Ni^{2+} in the electrolyte, ~2 µmol/g C_2H_4 are evolved during the first cycle (see green lines in Figure 3b), without any further C_2H_4 evolution in the subsequent cycles. If we compare the additional C_2H_4 evolution over 4 charge/discharge cycles induced by the presence of Ni^{2+} in the electrolyte on pristine graphite electrodes (~36 µmol/g; green line in Figure 1b) vs. on preformed graphite electrodes (~2 µmol/g; green line in Figure 3b), it becomes apparent that the effect of Ni^{2+} in the electrolyte is greatly suppressed by the presence of an SEI. Besides, also the additional reduction peaks between 2.5–1.5 V vs Li^+/Li seen in Figure 1a (green line) are no longer observed on the preformed graphite electrode (green line in Figure 3a). This suggests that nickel ions released into the electrolyte from cathode active materials over the course of extended charge/discharge cycling should hardly compromise the stability of the SEI, and thus should only have a very minor negative impact on the active lithium inventory of the cell.

On the contrary, the addition of 1.5 µmol Mn^{2+} to a graphite electrode preformed in EC/$LiPF_6$ (yellow lines in Figure 3) leads to a ~20-fold higher C_2H_4 evolution in the first cycle (39 µmol/g) compared to Ni^{2+}, which continues in subsequent cycles, accumulating to a total amount of evolved C_2H_4 of ~69 µmol/g after 4 cycles. This amounts to ~80% of the additional C_2H_4 evolved on a pristine graphite electrode upon the addition of Mn^{2+} ions to the electrolyte (see difference between blue and yellow lines in Figure 1), which therefore implies that even if the SEI is formed in an Mn^{2+}-free electrolyte, it is not able to suppress the detrimental electrolyte reduction reactions triggered by Mn^{2+} ions. In summary, while an SEI preformed in EC/$LiPF_6$ almost completely suppresses the negative effect of Ni^{2+} ions on electrolyte decomposition, it is not very effective in the presence of Mn^{2+} ions.

To better understand the effect of the SEI on the reactions caused by Mn^{2+} ions, we used the same graphite preformation procedure, but replaced the electrolyte for formation with DMC/$LiPF_6$ + 2 wt% vinylene carbonate (VC). In this case, the SEI formed with VC consists mainly of poly(VC) and Li_2CO_3,[69] and has been reported to partially mitigate the poor coulombic efficiency[70] and impedance growth[35] caused by transition metal ions; furthermore, due to the absence of EC, no LEDC is being formed.[62] After formation (2 cycles at C/8, yielding a cumulative irreversible capacity of ~31 mAh/g), the electrode was rinsed with pure DMC to remove any remaining VC, and was transferred into the 2-compartment OEMS cell. The orange lines in Figure 3 show the current profile and the C_2H_4 evolution of the VC-preformed graphite electrode cycled in EC/$LiPF_6$ + 1.5 µmol Mn^{2+} electrolyte. Although C_2H_4 is still evolved throughout all 4 cycles, its overall amount after 4 cycles is only ~20% of that obtained with the graphite electrode preformed in EC/$LiPF_6$ electrolyte (viz., 14 µmol/g vs. 69 µmol/g, comparing the orange vs. the yellow lines in Figure 3).

Figure 4a shows the evolution of C_2H_4, H_2, and CO after 4 cycles from all the experiments shown in Figure 3. The gas evolution in the TM-free electrolyte (blue bar) is limited to low amounts of H_2 (~7 µmol/g), probably from the reduction of newly introduced HF or trace water of the fresh electrolyte, its reduction largely perhibited by the preformed SEI. All of the TM-containing electrolytes evolve more H_2 (~23 µmol/g (Ni^{2+}) and ~32 µmol/g (Mn^{2+}) for electrodes preformed in EC/$LiPF_6$; ~28 µmol/g (Mn^{2+}) for electrodes preformed in DMC/2%VC/$LiPF_6$), suggesting that TM ions can catalyze the reduction of protic species, which is normally hindered by the SEI.[64] While for the electrode cycled in Ni^{2+}-containing electrolyte (green bars), only traces of CO (~1 µmol/g) are observed, the Mn^{2+}-containing electrolyte evolves ~32 µmol/g CO after 4 cycles if preformed in EC/$LiPF_6$ (yellow bars), lowered to ~12 µmol/g CO if preformed in DMC/2%VC/$LiPF_6$ (orange bars).

The corresponding cumulative irreversible capacity for the preformed electrodes after 4 cycles is displayed in Figure 4b. As expected from the gas evolution, the electrode cycled in the TM-free electrolyte (blue bars) shows the lowest irreversible capacity (~6 mAh/g). For the Ni^{2+}-containing electrolyte (green bars), the cumulative irreversible capacity is ~13 mAh/g, so that the excess irreversible loss (~7 mAh/g) is rather close to the theoretical capacity required for the 2-electron reduction of all Ni^{2+} ions (~7.5 mAh/g, see above). The highest irreversible capacity (~29 mAh/g) comes from the electrode preformed in EC and cycled in Mn^{2+}-containing electrolyte (yellow bars). The excess irreversible capacity measured for the EC/$LiPF_6$ preformed electrode caused by Mn^{2+} (~23 mAh/g more than in the TM-free electrolyte) is comparable to the additional irreversible capacity in

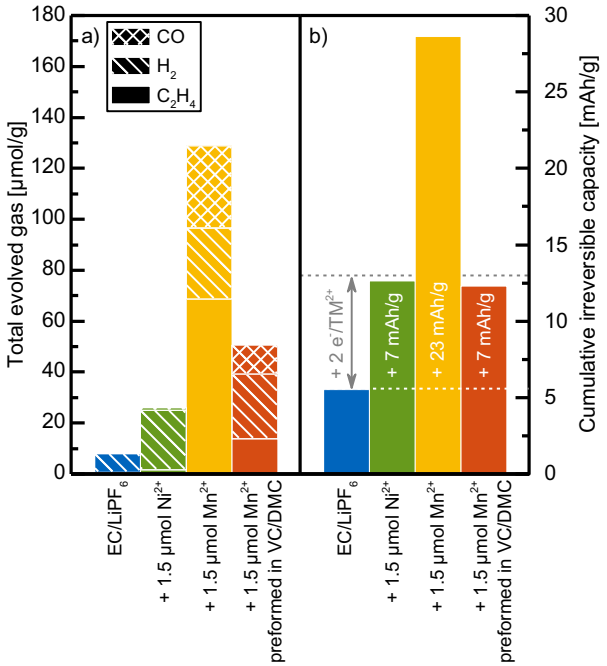

Figure 4. Total evolved gas and cumulative irreversible capacity (both normalized to graphite mass) over the first 4 cycles of the preformed graphite electrodes in EC/+1.5 M $LiPF_6$ with/without added metal salts, as shown in Figure 3. a) Total evolved C_2H_4 (solid bars), H_2 (dashed bars), and CO (squared bars). b) Cumulative irreversible capacity, with the gray arrow indicating the theoretical charge for 2-electron reduction of the added Ni^{2+} or Mn^{2+} ions. Preformation was done in two different electrolytes: i) EC/1.5 M $LiPF_6$ for the OEMS experiments in TM-free electrolyte (blue) or electrolyte with either 1.5 µmol $Ni(TFSI)_2$ (green lines) or 1.5 µmol $Mn(TFSI)_2$ (yellow); ii) DMC/1.5 M $LiPF_6$ + 2% VC for the OEMS experiment in electrolyte with 1.5 µmol $Mn(TFSI)_2$ (orange).

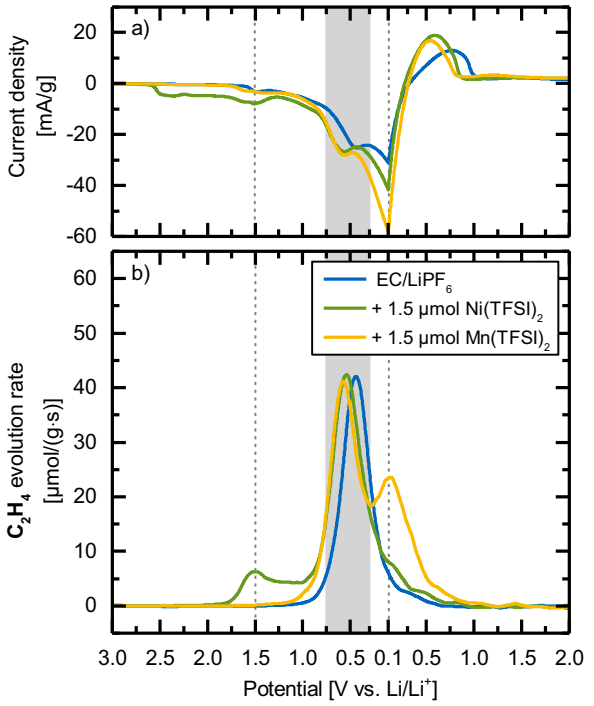

Figure 5. Currents and ethylene evolution rate during the first voltammetric cycle of pristine graphite electrodes in EC/1.5 M $LiPF_6$ electrolyte without added metal salts (blue lines), with 1.5 µmol $Ni(TFSI)_2$ (green lines), or with 1.5 µmol $Mn(TFSI)_2$ (yellow lines). a) Currents normalized to graphite mass (solid lines) and potential (red dashed line); b) integral ethylene evolution normalized to graphite mass. The data are extracted from Figure 1.

the experiment with pristine electrodes (~26 mAh/g, see yellow bars in Figure 2b), in agreement with the similar additional total gas evolution (C_2H_4 + H_2 + CO with respect to the TM-free electrolyte) of ~120 µmol/g on preformed electrodes (see yellow bars in Figure 4a) and ~121 µmol/g on pristine electrodes (see yellow bars in Figure 2a). On the contrary, the electrode preformed in DMC/$LiPF_6$ + 2%VC and cycled in an electrolyte with Mn^{2+} ions (orange bars in Figure 4b) shows a largely reduced irreversible capacity that is only ~7 mAh/g higher compared to the ~6 mAh/g obtained in the TM-free electrolyte, and thus this difference is very close again to the theoretical capacity required for the 2-electron reduction of all Mn^{2+} ions (~7.5 mAh/g, see above). While this additional capacity found for DMC/$LiPF_6$ + 2%VC preformed graphite in Mn^{2+}-containing electrolyte is identical to that for Ni^{2+}-containing electrolyte for EC/$LiPF_6$ preformed graphite (compare orange vs. green bars in Figure 4b), the additional amount of gas produced in the presence of Mn^{2+} ions is substantially larger (~44 µmol/g vs. ~16 µmol/g; compare orange vs. green bars in Figure 4a) compared to Ni^{2+}, suggesting that Mn^{2+} ions more effectively catalyze SEI and/or solvent reduction.

The results of Figure 3 and Figure 4 show that the activity of Ni^{2+} ions toward electrolyte reduction is suppressed by an EC-derived SEI, but that this SEI does not lead to significantly less side reactions for a Mn^{2+}-containing electrolyte. Hence, the dissolution of manganese will be far more detrimental toward long-term cell performance compared to that of nickel, which has previously been observed by Gilbert et al.[7] and Jung et al.[5] However, additives like VC can help to mitigate the detrimental effect of manganese, as apparently the SEI composition plays a crucial role on the reactivity of manganese toward electrolyte reduction.

Discussion

In order to obtain further insights into the effect of dissolved transition metals on the formation, the passivating properties, and the stability of the SEI on graphite electrodes, we will initially examine the very first voltammetric reduction and oxidation cycle on a pristine graphite electrode. Figure 5 magnifies the current density and plots the C_2H_4 evolution rate (obtained by taking the derivative of the integral OEMS signals) vs. the graphite potential for the first voltammetric cycle shown in Figure 1b. For the TM-free electrolyte (see blue lines in Figures 5a and 5b), the first main reduction peak is observed at ~0.5 V vs. Li^+/Li, which coincides with a maximum in ethylene evolution rate (see gray-shaded area in Figure 5). This peak appears for all three electrolytes and is ascribed to the reduction of EC to lithium ethylene dicarbonate (LEDC) and C_2H_4 on graphite.[51,52,55,59–63]

The electrolyte containing 1.5 µmol Ni^{2+} ions (green lines in Figure 5) shows an additional reduction current already at ~2.5 V vs. Li^+/Li, merging into a second small reduction current peak at ~1.5 V vs. Li^+/Li that is accompanied by a first peak in the C_2H_4 evolution rate. Jung et al.[5] observed the reduction of Ni^{2+} in a carbonate-based electrolyte at ~2.22 V vs. Li^+/Li, so that we ascribe the first reduction peak in the Ni-containing electrolyte at ~2.5 V vs. Li^+/Li (green line in Figure 5a) to the onset of Ni^{2+} reduction. By up-integrating the current density difference between the Ni-containing and the TM-free electrolyte during this initial part of the first reduction scan, it becomes apparent that the ~7.5 mAh/g needed for the reduction of Ni^{2+} to Ni^0 are only reached at ~1.4 V vs. Li^+/Li, which suggests that also the second peak around 1.5 V vs. Li^+/Li belongs to the reduction of Ni^{2+}. The concurrent C_2H_4 evolution initiating at below ~1.8 V vs. Li^+/Li is likely related to a reduction of EC on the nascent Ni^0 surface, which occurs apparently at higher potentials than the EC reduction on the graphite surface in TM-free EC/$LiPF_6$ electrolyte (blue line in Figure 5b), initiating at ~0.9 V vs. Li^+/Li (the same onset potential for C_2H_4 formation was observed for EC/EMC (3/7) with 1 M $LiPF_6$[52] or 1 M LiTFSI).[64] Interestingly, after the first two

reduction peaks (i.e., at 1.25 V vs. Li^+/Li), the integrated current accounts to ~7.9 mAh/g, whereas the charge required for the two-electron reduction of the formed C_2H_4 (11.8 μmol/g ≡ 0.63 mAh/g) and CO (9.3 μmol/g ≡ 0.50 mAh/g) together with the reduction of Ni^{2+} to Ni^0 (7.5 mAh/g) would require a total charge of ~8.6 mAh/g. This suggests that some of the electrolyte must have been reduced chemically rather than electrochemically, possibly via the re-oxidation of Ni^0 back to Ni^{2+} in a similar mechanism as suggested for manganese.[33,39]

When Mn^{2+} ions are added (see yellow lines in Figure 5), no additional current peak can be seen, even though the onset for C_2H_4 evolution (~1.1 V) is shifted ~0.2 V more positively compared the TM-free electrolyte. Since the onset for Mn^{2+} reduction was reported to occur at ~1.29 V vs. Li+/Li,[5] the more positive onset for C_2H_4 evolution in Mn^{2+}-containing electrolyte compared to TM-free electrolyte suggests that EC reduction is catalyzed by Mn° formed at the graphite electrode. Overall, these results with Ni^{2+}- and Mn^{2+}-containing electrolyte indicate that the earlier onset of C_2H_4 evolution occurs only below the respective reduction potential of the transition metal ions, suggesting that only the reduced transition metals are active toward electrolyte reduction. Rather noteworthy in the case of Mn^{2+}-containing electrolyte is that the C_2H_4 evolution rate increases again during the first positive-going potential scan, with a maximum at ~0.1 V vs. Li^+/Li (see gray dashed line at 0.1 V vs. Li^+/Li in Figure 5), in stark contrast to the vanishing C_2H_4 evolution rate in TM-free or Ni_{2+}-containing electrolyte. This is a clear evidence for the SEI decomposing properties of Mn^{2+} in contrast to Ni^{2+}.

That transition metals can affect the composition and stability of the SEI on graphite was proposed, e.g., by Joshi et al.,[32] who added 10 mM concentrations of each Ni^{+2}, Mn^{2+}, and Co^{2+} to a EC/DEC/$LiPF_6$ electrolyte and found evidence that transition metal ions catalyze the decomposition of LEDC in the SEI to Li_2CO_3, presumably by the release of C_2H_4, CO_2, and O_2. Later on, Leung[50] proposed that Mn^{2+} trapped in the SEI could decompose LEDC to alkoxides by releasing CO_2^-, which could convert to CO_2 by transferring the excess electron to a solvent molecule. This is consistent with the catalytic effect of Mn^{2+} on SEI decomposition deduced from Figure 3 and Figure 4, where continuous electrolyte decomposition even on a preformed graphite electrode is observed in the presence of Mn^{2+} ions. To better understand how transition metal ions in the electrolyte affect the SEI composition on a preformed electrode (in a TM-free EC/$LiPF_6$ electrolyte according to the above described procedure), they were transferred without washing into a new cell which we assembled with a fresh separators, a capacitively oversized LFP counter electrode, and an EC/$LiPF_6$ electrolyte with 1.5 μmol Mn^{2+} ions, 1.5 μmol Ni^{2+} ions, or without any transition metals. Subsequently, the cells were cycled between 2.0–3.45 V_{cell} at C/8 for two cycles, after which the harvested graphite electrodes were washed with DMC and then investigated by attenuated total reflection Fourier-transform infrared (ATR-FTIR) spectroscopy.

Figure 6 shows the ATR-FTIR spectra of the pristine (i.e., unused) graphite electrodes (gray spectra) as well as preformed electrodes cycled in the TM-free (blue spectra), Ni^{2+}-containing (green spectra), or Mn^{2+}-containing (yellow spectra) electrolyte. All spectra were normalized to have the same intensity for the PVDF peak at 1190 cm^{-1}, marked by the gray dashed line. For the cycled electrodes, the new peaks arising at ~1630 cm^{-1} and 1300 cm^{-1} can be assigned to LEDC,[71,72] whereas the peak at ~1750 cm^{-1} belongs to organic carbonate oligomers.[52] While no major differences could be found between the electrodes cycled in a TM-free and in an electrolyte with Ni^{2+} ions, the electrode cycled in the Mn^{2+}-containing electrolyte shows strongly pronounced peaks around 1420-1480 cm^{-1} (marked by the navy colored dashed lines), which is characteristic for inorganic carbonates like Li_2CO_3; for comparison, the spectra of pure Li_2CO_3 is also given in Figure 6 (navy line). Unfortunately, the Li_2CO_3 peak at ~850 cm^{-1} coincides with a PVDF peak (see gray line in Figure 6). Nevertheless, these results indicate that a Mn^{2+}-contaminated SEI contains more inorganic carbonates, in agreement with Joshi et al.[32] It is to note that this observation also fits to the mechanism proposed

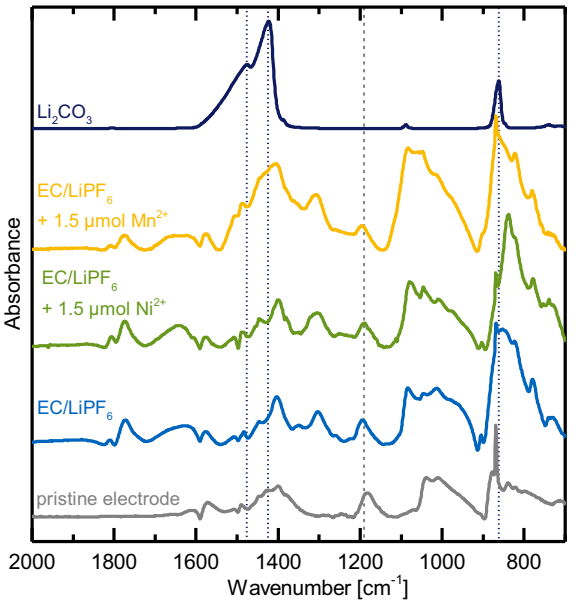

Figure 6. ATR-FTIR-spectra of a pristine graphite electrode (gray line) and of preformed graphite electrodes after two cycles at C/8 between 2.0–3.45 V_{cell} (in a cell with an LFP cathode) in different EC/1.5 M $LiPF_6$ electrolytes: i) without transition metal (blue line); ii) with 1.5 μmol $Ni(TFSI)_2$ (green line); or, iii) with 1.5 μmol $Mn(TFSI)_2$ (yellow line). Preformation was done in TM-free EC/1.5 M $LiPF_6$ for two cycles at C/8; prior to ATR-FTIR analysis, the cycled electrodes were washed with DMC. The spectra were normalized to the PVDF peak at 1190 cm^{-1} (see gray dashed line). The reference spectrum of Li_2CO_3 is also given, with characteristic peaks marked by the navy colored dotted lines.

by Leung,[50] as CO_2 (or CO_2^-) is readily reduced on graphite to form Li_2CO_3,[73] but due to the simultaneous consumption and evolution of CO_2 in our closed-cell system, this process would not be traceable by OEMS.

As both the reduction of EC and the decomposition of LEDC to Li_2CO_3 as proposed by Joshi et al.[32] would lead to the evolution of C_2H_4, we designed an experiment where these two processes could be separated. For this, we carefully washed graphite electrodes preformed in TM-free EC/$LiPF_6$ with 5 mL DMC, and then cycled them in the 2-compartment OEMS cell with DMC/$LiPF_6$ electrolyte containing either 1.5 μmol Mn^{2+} ions or no TM ions. As the reduction of DMC generates CO, but no C_2H_4,[66] we should now be able to differentiate between electrolyte reduction and SEI decomposition. To first test if any EC remains in the pores of the electrode after washing, we additionally soaked a graphite electrode with the EC/$LiPF_6$ electrolyte, rinsed it, and then cycled it in the TM-free DMC/$LiPF_6$ electrolyte. Figure 7 shows the current density (a) and the C_2H_4 evolution (b) over the course of 4 voltammetric cycles. The electrode that was stored in EC/$LiPF_6$ and cycled in DMC/$LiPF_6$ shows a strong CO evolution (dashed navy colored line), amounting to ~148 μmol/g CO over 4 cycles, as no passivating SEI layer is present; these results are similar to a previous gas evolution study on EMC/$LiPF_6$ electrolytes by our group, where CO is the only gas evolved upon the reduction of EMC.[55] However, for the EC/$LiPF_6$ soaked graphite electrode, ~11 μmol/g C_2H_4 (solid navy colored line) are evolved over the 4 cycles, which originate from the remaining EC that could not be removed by the washing step (however, still a minor amount compared to the evolved CO). In contrast, the preformed electrode that was cycled in the TM-free DMC/$LiPF_6$ electrolyte (superimposing blue solid and dashed lines in Figure 7) shows neither CO nor C_2H_4 (<0.1 μmol/g), meaning that the SEI has not been damaged due to the washing process.

Lastly, the yellow lines in Figure 7 show the behavior of the preformed graphite electrode cycled in the Mn^{2+}-containing DMC/$LiPF_6$ electrolyte. In this case, both CO and C_2H_4 are evolved throughout

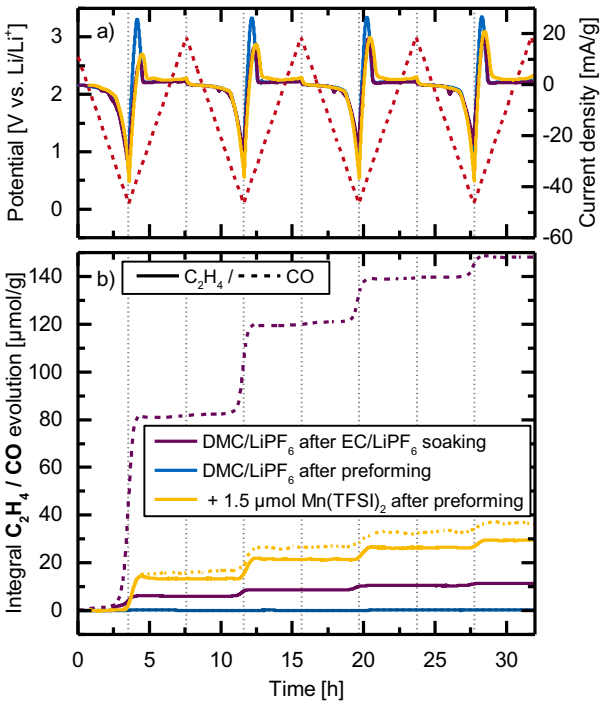

Figure 7. a) Currents normalized to graphite mass and b) evolution of ethylene (solid lines) and CO (dashed lines) during the first 4 voltammetric cycles of preformed graphite electrodes in DMC/1.5 M $LiPF_6$ electrolyte without (blue lines) and with 1.5 µmol Mn^{2+} ions (yellow lines). Preformation was done with TM-free EC/1.5 M $LiPF_6$ electrolyte in a separate cell vs. an LFP cathode (2 cycles at C/8); harvested electrodes were washed with DMC prior to building the 2-compartment OEMS cells. To determine the efficacy of the washing procedure, a pristine graphite electrode soaked in EC/1.5 M $LiPF_6$ electrolyte and then washed was also examined (dark purple lines). The voltammetric cycles at 0.2 mV/s were done between 0.1–3.0 V vs. Li^+/Li, starting from OCV (~2.9 V vs. Li^+/Li).

all 4 cycles. As the C_2H_4 evolution from the Mn^{2+}-containing electrolyte is ~30 µmol/g after 4 cycles (see solid yellow line in Figure 7b) while the EC residuals from the EC-soaked electrode account to only ~11 µmol/g C_2H_4 (see solid navy line in Figure 7b), we hypothesize that this additional ~19 µmol/g C_2H_4 originate from the decomposition of LEDC. This LEDC-derived amount of C_2H_4 may be compared to the higher amount of ~69 µmol/g C_2H_4 evolved for an identically preformed graphite electrode but cycled in EC/$LiPF_6$ + Mn^{2+} (Figure 3b, yellow lines). From this it becomes clear that the Mn catalyzed LEDC decomposition must compromise the integrity of the SEI, so that further electrolyte reduction can occur, namely of EC to C_2H_4 in the EC/$LiPF_6$ electrolyte. This hypothesis is confirmed by the strong CO evolution upon cycling of preformed graphite electrodes in the Mn^{2+}-containing DMC/$LiPF_6$ electrolyte (dashed yellow line in Figure 7b), where a major fraction of the evolved gas is produced by the direct reduction of DMC to CO. In summary, the comparison of the gas evolution of graphite electrodes preformed in EC/$LiPF_6$ and then cycled in Mn^{2+}-containing EC/$LiPF_6$ (Figure 3b) vs. Mn^{2+}-containing DMC/$LiPF_6$ (Figure 7b) reveals that the Mn catalyzed LEDC decomposition of LEDC must be leading to morphological changes in the SEI which leads to further electrolyte decomposition.

Based on our here presented results and numerous previous studies, we suggest the following mechanism for the catalytic decomposition of electrolyte by manganese ions, which is sketched in Scheme 1: After the Mn^{2+} ions are absorbed into the SEI by ion exchange (process (1) in Scheme 1), they diffuse through the SEI until they are close enough for an electron transfer from the lithiated graphite via tunneling, which leads to the deintercalation of lithium from graphite (2). If the reduced manganese is surrounded by LEDC, the latter is reduced to Li_2CO_3 and C_2H_4, while the manganese is simultaneously oxidized back to

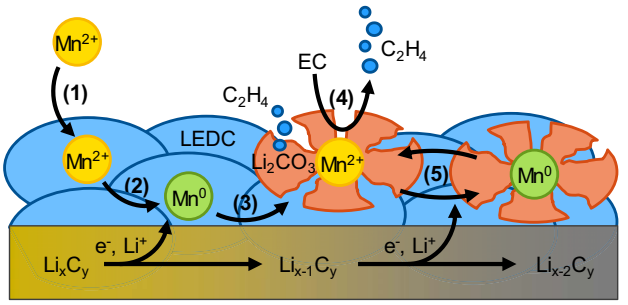

Scheme 1. Proposed mechanism for the continuous decomposition of SEI and electrolyte as monitored by C_2H_4 evolution for a preformed electrode with a Mn^{2+}-containing electrolyte (see text for details): (1) Absorption of Mn^{2+} ions into the SEI; (2) reduction of Mn^{2+} ions in the SEI and deintercalation of Li^+ from graphite; (3) re-oxidation of Mn^0 to Mn^{2+}; (4) recurrent electrolyte reduction; (5) catalytic cycle of electrolyte decomposition.

Mn^{2+} (3). Alternatively, LEDC could be reduced to lithium alkoxides and CO_2^- as suggested by Leung,[50] eventually also forming Li_2CO_3. The reduction contracts the SEI in the vicinity, leading to cracks which are filled with fresh electrolyte. This electrolyte will be reduced (4), and, if EC-based, produce additional C_2H_4. Consequently, Mn^{2+} would be located at the border between organic and inorganic SEI, in agreement with previous observations.[25,32,37,38] The Mn^{2+} ion can now accept further electrons and pass them on to surrounding LEDC or EC molecules (5), thereby leading to a catalytic cycle of electrolyte decomposition and active lithium loss from the lithiated graphite. This cycle can continue until the Mn^{2+} ion is eventually fully encapsulated by non-reducible decomposition products, so that an electron transfer from the lithiated graphite is no longer feasible. As Wandt et al.[4] found manganese almost exclusively in its 2+ oxidation state by operando XAS, the re-oxidation of Mn^0 to Mn^{2+} must be faster than the reduction of Mn^{2+}, i.e., the diffusion within the SEI and the electron transfer (steps 2 and 5 in Scheme 1) are the rate-limiting steps.

While both nickel and manganese have shown activity toward electrolyte decomposition in their reduced state (i.e., on pristine electrodes, see Figure 1), the presence of a preformed SEI greatly suppressed the effect of Ni^{2+}containing electrolyte on both gas evolution (see Figure 3b, green line) and the enrichment of Li_2CO_3 in the SEI (see Figure 6, green line). Hence, we can assume that the diffusion and/or the electron transfer of Ni^{2+} within the SEI is slowed down compared to Mn^{2+}. As suggested by Shkrob et al.,[38] it is possible that nickel and manganese are not fully reduced, but only one electron is transferred through the SEI to the transition metal ion. DFT-calculations by Leung[50] indicate that a Ni(I) species is far less likely to transfer an electron to neighboring SEI molecules compared to its Mn(I) counterpart. In this case, the catalytic cycle for Ni would be effectively interrupted. Additionally, Wandt et al.[4] found that Mn^{2+} in the SEI is reduced within minutes once the electrolyte is completely removed, whereas nickel stays in its 2+ state. As the reduction potential of Ni^{2+}/Ni is ~1 V higher than the reduction potential of Mn^{2+}/Mn,[5,74] the electron transfer from lithiated graphite to Ni^{2+} should have a higher thermodynamic driving force. Hence, another possible reason for the apparent difference between Ni and Mn is that the Li^+/Ni^{2+} exchange and the diffusion of Ni^{2+} within the SEI is much slower compared to Mn^{2+}.

For Li-ion batteries, this has two implications: i) The same amount of TM dissolution leads to less severe capacity fading if the cathode active material is Ni-rich and Mn-poor, which is advantageous for Ni-rich NMCs and especially Mn-free NCA (as seen by Gilbert et al.[7]); ii) future additive design should focus on the formation of an SEI which enables Li^+ ion transport while slowing down the diffusion of all transition metal ions, or which form SEI products which consist of chemically stable species that cannot be further reduced. In this context, a thermally aged SEI that contains more LiF and other

stable inorganic species[75] might be more robust toward the detrimental side reactions induced by manganese ions. However, as Mn^{2+} rapidly exchanges with Li^+ from LiF in the SEI,[25,37] a high LiF content will likely not act as a barrier for Mn^{2+} diffusion.

Conclusions

In this work, we applied on-line electrochemical mass spectrometry (OEMS) to follow the reactions triggered by manganese and nickel that ultimately lead to the loss of active lithium and poor capacity retention in full-cells. For the first time, we have investigated the effect of Mn^{2+} and Ni^{2+} on the gassing behavior of graphite, using EC/$LiPF_6$ model electrolytes with $Mn(TFSI)_2$ or $Ni(TFSI)_2$ in a 2-compartment cell. Both manganese and nickel significantly increase the C_2H_4 evolution and thus ethylene carbonate (EC) reduction on pristine graphite electrodes. Furthermore, the Mn^{2+}-containing electrolyte showed an ongoing EC reduction and C_2H_4 evolution throughout several cycles after formation.

As a second step, we investigated the effect of Mn^{2+} and Ni^{2+} on graphite electrodes which already featured an SEI by preforming them in a TM-free electrolyte. We found that the effect of nickel is greatly suppressed by the SEI, whereas manganese showed almost the same activity toward electrolyte reduction as on pristine electrodes. However, a preformation in a VC-containing electrolyte could significantly lower the side reactions caused by Mn^{2+} ions. As this showed that the SEI chemistry plays a crucial role, we found by post-mortem ATR-FTIR spectroscopy that the graphite electrodes cycled in an Mn^{2+}-containing electrolyte consisted of more Li_2CO_3 compared to electrodes cycled in an electrolyte with Ni^{2+} ions or no transition metals. Further OEMS experiments with preformed graphite electrodes and a DMC electrolyte (which allowed us to distinguish between electrolyte reduction and SEI decomposition) indicated that Mn^{2+} leads to the decomposition of LEDC to C_2H_4 and Li_2CO_3; however, the major part of the gas evolution still originated directly from the electrolyte reduction. Our results suggest that cathode active materials with low or zero manganese contents should be advantageous with respect to the detrimental effects of transition metal dissolution, and that SEI-stabilizing additives can be an efficient way to decrease the side reactions caused by transition metal ions in Li-ion batteries.

Acknowledgments

Sophie Solchenbach gratefully acknowledges the BASF Battery Research Network for financial support. Funding for Roland Jung was provided by BMW AG. The authors thank Prof. Brett Lucht for fruitful discussions.

ORCID

Sophie Solchenbach https://orcid.org/0000-0001-6517-8094
Roland Jung https://orcid.org/0000-0003-1135-7438

References

1. Y. Terada, Y. Nishiwaki, I. Nakai, and F. Nishikawa, *J. Power Sources*, **97–98**, 420 (2001).
2. H. Tsunekawa, S. Tanimoto, R. Marubayashi, M. Fujita, K. Kifune, and M. Sano, *J. Electrochem. Soc.*, **149**, A1326 (2002).
3. D. H. Jang, Y. J. Shin, and S. M. Oh, *J. Electrochem. Soc.*, **143**, 2204 (1996).
4. J. Wandt, A. Freiberg, R. Thomas, Y. Gorlin, A. Siebel, R. Jung, H. A. Gasteiger, and M. Tromp, *J. Mater. Chem. A*, **4**, 18300 (2016).
5. R. Jung, F. Linsenmann, R. Thomas, J. Wandt, S. Solchenbach, F. Maglia, C. Stinner, M. Tromp, and H. A. Gasteiger, *manuscript in preparation* (2018).
6. H. Zheng, Q. Sun, G. Liu, X. Song, and V. S. Battaglia, *J. Power Sources*, **207**, 134 (2012).
7. J. A. Gilbert, I. A. Shkrob, and D. P. Abraham, *J. Electrochem. Soc.*, **164**, 389 (2017).
8. D. R. Gallus, R. Schmitz, R. Wagner, B. Hoffmann, S. Nowak, I. Cekic-Laskovic, R. W. Schmitz, and M. Winter, *Electrochim. Acta*, **134**, 393 (2014).
9. I. Buchberger, S. Seidlmayer, A. Pokharel, M. Piana, J. Hattendorff, P. Kudejova, R. Gilles, and H. A. Gasteiger, *J. Electrochem. Soc.*, **162**, A2737 (2015).
10. D. P. Abraham, T. Spila, M. M. Furczon, and E. Sammann, *Electrochem. Solid-State Lett.*, **11**, A226 (2008).
11. X. Liao, Q. Huang, S. Mai, X. Wang, M. Xu, L. Xing, Y. Liao, and W. Li, *J. Power Sources*, **286**, 551 (2015).
12. M. Metzger, B. Strehle, S. Solchenbach, and H. A. Gasteiger, *J. Electrochem. Soc.*, **163**, A798 (2016).
13. S. Solchenbach, M. Metzger, M. Egawa, H. Beyer, and H. A. Gasteiger, *J. Electrochem. Soc.*, **165**, A3022 (2018).
14. T. Li, L. Xing, W. Li, Y. Wang, M. Xu, F. Gu, and S. Hu, *J. Power Sources*, **244**, 668 (2013).
15. O. Borodin, W. Behl, and T. R. Jow, *J. Phys. Chem. C*, **117**, 8661 (2013).
16. D. H. Jang and S. M. Oh, *J. Electrochem. Soc.*, **144**, 3342 (1997).
17. K. Amine, J. Liu, S. Kang, I. Belharouak, Y. Hyung, D. R. Vissers, and G. L. Henriksen, *J. Power Sources*, **129**, 14 (2004).
18. R. Jung, M. Metzger, F. Maglia, C. Stinner, and H. A. Gasteiger, *J. Electrochem. Soc.*, **164**, A1361 (2017).
19. R. Jung, M. Metzger, F. Maglia, C. Stinner, and H. A. Gasteiger, *J. Phys. Chem. Lett.*, **8**, 4820 (2017).
20. J. Wandt, A. Freiberg, A. Ogrodnik, and H. A. Gasteiger, *Mater. Today*, in press (2018).
21. D. Streich, C. Erk, A. Gue, P. Mu, F.-F. Chesneau, and E. J. Berg, *J. Phys. Chem. C*, **121**, 13481 (2017).
22. D. Streich, A. Guéguen, M. A. Mendez, F. F. Chesneau, P. Novák, and E. J. Berg, *J. Electrochem. Soc.*, **163**, A964 (2016).
23. A. Freiberg, S. Solchenbach, B. Strehle, A. Siebel, M. Tromp, and H. A. Gasteiger, *ECS Meet. Abstr.*, **2**, 179 (2018).
24. C. Zhan, J. Lu, A. J. Kropf, T. Wu, A. N. Jansen, Y. K. Sun, X. Qiu, and K. Amine, *Nat. Commun.*, **4**, 2437 (2013).
25. D. R. Vissers, Z. Chen, Y. Shao, M. H. Engelhard, U. Das, P. C. Redfern, L. A. Curtiss, B. Pan, J. Liu, and K. Amine, *ACS Appl. Mater. Interfaces*, **8**, 14244 (2016).
26. W. Choi and A. Manthiram, *J. Electrochem. Soc.*, **153**, A1760 (2006).
27. C. Zhan, T. Wu, J. Lu, and K. Amine, *Energy Environ. Sci.*, **11**, 243 (2018).
28. T. Tsujikawa, K. Yabuta, and T. Matsushita, *J. Electrochem. Soc.*, **158**, 322 (2011).
29. N. P. W. Pieczonka, Z. Liu, P. Lu, K. L. Olson, J. Moote, B. R. Powell, and J. Kim, *J. Phys. Chem. C*, **117**, 15947 (2013).
30. L. M. Thompson, W. Stone, A. Eldesoky, N. K. Smith, C. R. M. Mcfarlane, J. S. Kim, M. B. Johnson, R. Petibon, and J. R. Dahn, **165**, 2732 (2018).
31. S. Komaba, N. Kumagai, and Y. Kataoka, *Electrochim. Acta*, **47**, 1229 (2002).
32. T. Joshi, K. Eom, G. Yushin, and T. F. Fuller, *J. Electrochem. Soc.*, **161**, A1915 (2014).
33. M. Ochida, Y. Domi, T. Doi, S. Tsubouchi, H. Nakagawa, T. Yamanaka, A. Abouimrane, and Z. Ogumi, *J. Electrochem. Soc.*, **159**, A961 (2012).
34. D. Pritzl, J. Landesfeind, S. Solchenbach, and H. A. Gasteiger, *J. Electrochem. Soc.*, **165**, A2145 (2018).
35. C. Zhan, X. Qiu, J. Lu, and K. Amine, *Adv. Mater. Interfaces*, **3**, 1500856 (2016).
36. Y. K. Lee, J. Park, and W. Lu, *J. Electrochem. Soc.*, **164**, 2812 (2017).
37. H. Shin, J. Park, A. M. Sastry, and W. Lu, *J. Power Sources*, **284**, 416 (2015).
38. I. A. Shkrob, A. J. Kropf, T. W. Marin, Y. Li, O. G. Poluektov, J. Niklas, and D. P. Abraham, *J. Phys. Chem. C*, **118**, 24335 (2014).
39. C. Delacourt, A. Kwong, X. Liu, R. Qiao, W. L. Yang, P. Lu, S. J. Harris, and V. Srinivasan, *J. Electrochem. Soc.*, **160**, A1099 (2013).
40. T. Nordh, S. R. Younesi, M. Hahlin, R. F. Duarte, C. Tengstedt, D. Brandell, and K. Edström, *J. Phys. Chem. C*, **120**, 3206 (2016).
41. S. Komaba, T. Itabashi, T. Ohtsuka, H. Groult, N. Kumagai, B. Kaplan, and H. Yashiro, *J. Electrochem. Soc.*, **152**, A937 (2005).
42. X. Xiao, Z. Liu, L. Baggetto, G. M. Veith, K. L. More, and R. R. Unocic, *Phys. Chem. Chem. Phys.*, **16**, 10398 (2014).
43. S. R. Gowda, K. G. Gallagher, J. R. Croy, M. Bettge, M. M. Thackeray, and M. Balasubramanian, *Phys. Chem. Chem. Phys.*, **16**, 6898 (2014).
44. M. J. Aragon, C. Pérez-Vicente, and J. L. Tirado, *Electrochem. commun.*, **9**, 1744 (2007).
45. S. Mirhashemihaghighi, B. Leo, C. Pe, J. L. Tirado, and E. M. Arroyo, *Inorg. Chem.*, **51**, 5554 (2012).
46. Y. T. Teng, S. S. Pramana, J. Ding, T. Wu, and R. Yazami, *Electrochim. Acta*, **107**, 301 (2013).
47. D. H. Lee, K. J. Carroll, K. W. Chapman, O. J. Borkiewicz, S. Calvin, E. E. Fullerton, and Y. S. Meng, *Phys. Chem. Chem. Phys.*, **16**, 3095 (2014).
48. K. Rui, Z. Wen, Y. Lu, J. Jin, and C. Shen, *Adv. Energy Mater.*, **5**, 1401716 (2015).
49. Y.-K. Han, K. Lee, S. Kang, Y. Suk, and H. Lee, *Comput. Mater. Sci.*, **81**, 548 (2014).
50. K. Leung, *Chem. Mater.*, **29**, 2550 (2016).
51. R. Imhof and P. Novák, *J. Electrochem. Soc.*, **145**, 1081 (1998).
52. B. Zhang, M. Metzger, S. Solchenbach, M. Payne, S. Meini, H. A. Gasteiger, A. Garsuch, and B. L. Lucht, *J. Phys. Chem. C*, **119**, 11337 (2015).
53. N. Tsiouvaras, S. Meini, I. Buchberger, and H. A. Gasteiger, *J. Electrochem. Soc.*, **160**, A471 (2013).
54. M. Metzger, C. Marino, J. Sicklinger, D. Haering, and H. A. Gasteiger, *J. Electrochem. Soc.*, **162**, A1123 (2015).
55. B. Strehle, S. Solchenbach, M. Metzger, K. U. Schwenke, and H. A. Gasteiger, *J. Electrochem. Soc.*, **164**, A2513 (2017).
56. Y. Peng and P. Wu, *Polymer (Guildf.)*, **45**, 5295 (2004).
57. D. Strmcnik, I. E. Castelli, J. G. Connell, D. Haering, M. Zorko, P. Martins, P. P. Lopes, B. Genorio, T. Østergaard, H. A. Gasteiger et al., *Nat. Catal.*, **1**, 255 (2018).
58. U. Heider, R. Oesten, and M. Jungnitz, *J. Power Sources*, 7 (1999).
59. D. Aurbach, Y. Gofer, M. Ben-Zion, and P. Aped, *J. Electroanal. Chem.*, **339**, 451 (1992).
60. M. Nie, D. Chalasani, D. P. Abraham, Y. Chen, A. Bose, and B. L. Lucht, *J. Phys. Chem. C*, **117**, 1257 (2013).

61. D. Aurbach, Y. Ein-Ely, and A. Zaban, *J. Electrochem. Soc.*, **141**, L1 (1994).
62. H. Ota, Y. Sakata, A. Inoue, and S. Yamaguchi, *J. Electrochem. Soc.*, **151**, A1659 (2004).
63. R. Bernhard, S. Meini, and H. A. Gasteiger, *J. Electrochem. Soc.*, **161**, A497 (2014).
64. R. Bernhard, M. Metzger, and H. A. Gasteiger, *J. Electrochem. Soc.*, **162**, A1984 (2015).
65. M. Onuki, S. Kinoshita, Y. Sakata, M. Yanagidate, Y. Otake, M. Ue, and M. Deguchi, *J. Electrochem. Soc.*, **155**, A794 (2008).
66. H. Yoshida, T. Fukunaga, T. Hazama, M. Terasaki, M. Mizutani, and M. Yamachi, *J. Power Sources*, **68**, 311 (1997).
67. K. Leung, *Chem. Phys. Lett.*, **568–569**, 1 (2013).
68. R. Mogi, M. Inaba, Y. Iriyama, T. Abe, and Z. Ogumi, *J. Power Sources*, **119–121**, 597 (2003).
69. A. L. Michan, B. S. Parimalam, M. Leskes, R. N. Kerber, T. Yoon, C. P. Grey, and B. L. Lucht, *Chem. Mater.*, **28**, 8149 (2016).
70. D. Pritzl, S. Solchenbach, M. Wetjen, and H. A. Gasteiger, *J. Electrochem. Soc.*, **164**, A2625 (2017).
71. L. Gireaud, S. Grugeon, S. Laruelle, S. Pilard, and J.-M. Tarascon, *J. Electrochem. Soc.*, **152**, A850 (2005).
72. D. M. Seo, D. Chalasani, B. S. Parimalam, R. Kadam, M. Nie, and B. L. Lucht, *ECS Electrochem. Lett.*, **3**, A91 (2014).
73. Y. Ein-Eli, B. Markovsky, D. Aurbach, Y. Carmeli, H. Yamin, and S. Luski, *Electrochim. Acta*, **39**, 2559 (1994).
74. P. Vanýsek, in *CRC Handbook of Chemistry and Physics*, W. Haynes, Editor, CRC Press LLC (2000).
75. B. S. Parimalam, A. D. Macintosh, R. Kadam, and B. L. Lucht, *J. Phys. Chem. C*, **121**, 22733 (2017).